EPJ manuscript No.
(will be inserted by the editor)

The reaction $\pi N \to \pi\pi N$ in a meson-exchange approach

S. Schneider[1] [a], S. Krewald[1], and Ulf-G. Meißner[1,2]

[1] Institut für Kernphysik, Forschungszentrum Jülich, D-52425 Jülich, Germany
[2] Universität Bonn, Helmholtz-Institut für Strahlen- und Kernphysik, Nußallee 14-16, D-53115 Bonn, Germany

Received: date / Revised version: date

Abstract. A resonance model for two-pion production in the pion-nucleon reaction is developed that includes information obtained in the analysis of pion-nucleon scattering in a meson-exchange model. The baryonic resonances $\Delta(1232)$, $N^*(1440)$, $N^*(1520)$, $N^*(1535)$, and $N^*(1650)$ are included. The model reproduces the total cross sections up to kinetic energies of the incident pion of 350 MeV and obtains the shapes of the differential cross sections in reasonable agreement with the data.

PACS. 13.75.-n Hadron-induced low- and intermediate-energy reactions – 13.75.Gx Pion-baryon interactions – 13.85.Fb Inelastic scattering:two-particle final states – 14.20.Gk Baryon resonances with S=0

1 Introduction

Recent experimental progress provides data for two-pion production in both pion-induced and electromagnetic reactions up to energies of about 2.1 GeV, see e.g. Refs. [1,2, 3,4,5]. New isobar models have been developed to deduce masses and widths of baryon resonances from the data [6, 7]. A basic problem for these analyses is given by the fact that the excitation of resonances is accompanied by other non-resonant processes, the so-called background. At present, the non-resonant processes are treated phenomenologically [6], using or extending methods known from the analysis of pion-nucleon scattering [8,9,10,11]. A combined theoretical treatment of resonances and background is a challenge for theory.

At low energies, chiral perturbation theory provides a quantitative theoretical understanding of pion-induced two-pion production. Calculations in heavy baryon chiral perturbation theory have been extended to third order [12,13,14]. An important result obtained in Ref. [13] is the observation that contributions from loop diagrams are negligible. This is non-trivial because in pion-nucleon scattering, unitarity effects can be important even close to threshold in some partial waves. In two-pion production, however, the imaginary contributions interfere destructively. The important contributions at third order are the tree level diagrams involving the finite dimension two low–energy constants c_i and tree level corrections of order $1/m_N$, with m_N the nucleon mass. This finding of Ref. [13] explains why a previous relativistic baryon chiral perturbation theory calculation at tree level including terms from the dimension two effective pion-nucleon Lagrangian works so well for pion kinetic energies up to 400 MeV [15]. Moreover, the numerical values of the low–energy constants (LECs) c_i of the pion-nucleon Lagrangian can be understood in terms of resonance saturation [16], more precisely through the s- and u-channel excitations of baryon resonances ($\Delta, N^*(1440)$) and t-channel meson resonances (σ, ρ). As a consequence, one may obtain a reasonable model for treating baryon resonances in two-pion production reactions by replacing the low–energy constants of chiral perturbation theory by diagrams containing explicit resonances. This has been done by Jensen and Miranda [17] and by Kammano and Arima [18] and in resonance models like e.g. [19,20,21,22]. Such an approach makes sense if one checks that at low energies the chiral perturbation theory results are recovered or if one enforces this behaviour through explicit matching of the pertinent amplitudes.

In the present work, we want to include information about pion-nucleon scattering into the construction of a resonance model for two-pion production. We use results obtained in Ref. [23] which treats pion-nucleon scattering in a coupled-channel model. The model incorporates the effects of the $\pi\pi N$ states by introducing σN, $\pi\Delta$ and ρN channels. The interactions between these channels is derived from an chirally symmetric Lagrangian supplemented by additional terms for the Δ, ω, ρ, and σ fields. The model includes the $\Delta(1232)$, $N^*(1520)$, $N^*(1535)$, and $N^*(1650)$ as explicit resonances. It is able to reproduce the experimental phase shifts and inelasticities up to 1500 MeV. For larger energies, it predicts a non-resonant background. The model does not need an explicit Roper resonance $N^*(1440)$, but is able to describe the P_{11} partial wave and in particular the inelasticity by the dynamics of the σN and $\pi\Delta$ channels.

[a] *Present address:* Carl Zeiss SMT AG, Oberkochen, Germany.

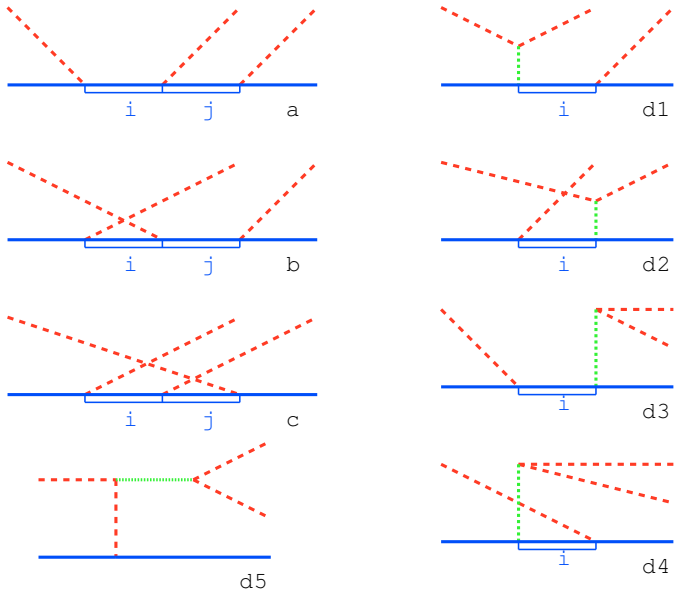

Fig. 1. Classes of diagrams describing the $\pi N \to \pi\pi N$ reaction near threshold. The internal baryon propagators labeled i and j (blue double lines) represent the nucleon, the Δ, and the N^* resonances $N^*(1440)$, $N^*(1520)$, $N^*(1535)$, $N^*(1650)$, respectively. The ρ and σ meson propagators are shown by (green) dotted lines. The (red) dashed lines stand for external pions, while (blue) solid lines are external nucleons.

2 The model

Fig. 1 shows the classes of diagrams which are included in the present resonance model. The diagrams (a), (b), and (c) contain two baryon propagators whereas (d1) - (d4) contain one. We consider the nucleon, the $\Delta(1232)$, and the $N^*(1520)$, $N^*(1535)$, $N^*(1650)$, and $N^*(1440)$ which are denoted by the indices i and j, respectively. We also include two–pion resonances in the $I_{\pi\pi} = 0$ and $I_{\pi\pi} = 1$ partial waves, see diagram (d5) (and below).

Meson-dynamical models generate unitary pion-nucleon scattering T-matrices by solving the Bethe-Salpeter equation

$$T = K + K\,G\,T, \tag{1}$$

where G denotes the two-particle propagator and K the scattering kernel which in principle includes all two-particle irreducible diagrams. The scattering kernel can be split into a pole term K_2 which contains s-channel pole diagrams and the non-pole term $K_1 = K - K_2$. As is well known, the T-matrix separates into a pole part T_2 and a non-pole part $T_1 = T - T_2$ [24,25]. The non-pole T-matrix is obtained by solving

$$T_1 = K_1 + K_1 G T_1 \ . \tag{2}$$

The non-pole T-matrix generates the dressed vertex f which is obtained from the bare vertex f_0 as follows:

$$f = f_0 + f_0\,G\,T_1 \ . \tag{3}$$

The self–energy Σ is given by

$$\Sigma = f_0^\dagger\,G\,f \ , \tag{4}$$

Table 1. The meson-baryon interaction Lagrangian.

vertex	$\mathcal{L}$
πNN	$-\frac{f_{\pi NN}}{M_\pi}\bar\psi\gamma_5\gamma_\mu\tau_a\partial^\mu\pi_a\psi$
$\pi N\Delta$	$\frac{f_{\pi N\Delta}}{M_\pi}\bar\Delta^\mu T_a^\dagger\partial^\mu\pi_a\psi$ + h.c.
$\rho\pi\pi$	$-g_{\rho\pi\pi}\epsilon_{abc}\pi_a\partial^\mu\pi_b\rho_c$
ρNN	$-g_{\rho NN}\bar\psi(\gamma_\mu - \frac{\kappa_{\rho NN}}{2m_N}\sigma^{\mu\nu}\partial_\nu)\tau_a\rho_\mu^a\psi$
$\sigma\pi\pi$	$-g_1 M_\pi^2\pi_a\pi_a\sigma + \frac{g_2}{2}\partial_\mu\pi_a\partial^\mu\pi_a\sigma$
σNN	$-g_{\sigma NN}\bar\psi\psi\sigma$
$\sigma\sigma\sigma$	$-g_{\sigma\sigma\sigma}M_\sigma\,\sigma^3$
$\pi\Delta\Delta$	$\frac{f_{\pi\Delta\Delta}}{M_\pi}\bar\Delta_\mu\gamma_5\gamma_\nu T_a\partial^\nu\pi_a\Delta^\mu$
$\rho N\Delta$	$-i\frac{f_{\rho N\Delta}}{M_\rho}\bar\Delta^\mu\gamma_5\gamma^\nu T_a^\dagger\rho^a_{\mu\nu}\psi + h.c.$
$\rho\Delta\Delta$	$-g_{\rho NN}\bar\Delta_\sigma(\gamma_\mu - \frac{\kappa_{\rho\Delta\Delta}}{2m_\Delta}\sigma^{\mu\nu}\partial_\nu)T_a\rho_\mu^a\Delta^\sigma$
$P_{11}\pi N$	$-\frac{f_{P_{11}\pi N}}{M_\pi}\bar\psi_{N^*}\gamma_5\gamma_\mu\tau_a\partial^\mu\pi_a\psi + h.c.$
$P_{11}\pi\Delta$	$\frac{f_{P_{11}\pi\Delta}}{M_\pi}\bar\Delta^\mu T_a^\dagger\partial_\mu\pi_a\psi_{N^*} + h.c.$
$P_{11}\sigma\Delta$	$-g_{P_{11}\sigma N}\bar\psi_{N^*}\psi\sigma + h.c.$
$D_{13}\pi N$	$i\frac{f_{D_{13}\pi N}}{M_\pi^2}\bar\psi^\mu_{N^*}\gamma_5\gamma^\nu\tau_a\psi\partial_\nu\partial_\mu\pi_a + h.c.$
$D_{13}\pi\Delta$	$\frac{f_{D_{13}\pi\Delta}}{M_\pi}\bar\psi^\mu_{N^*}\gamma_\nu T_a\partial^\nu\pi_a\Delta_\mu + h.c.$
$S_{11}\pi N$	$\frac{f_{S_{11}\pi N}}{M_\pi}\bar\psi_{N^*}\gamma_\mu\tau_a\partial^\mu\pi_a\psi + h.c.$
$S_{11}\eta N$	$\frac{f_{S_{11}\eta N}}{M_\eta}\bar\psi_{N^*}\gamma_\mu\partial^\mu\eta\psi + h.c.$

and the pole T-matrix reads

$$T_2 = f^\dagger\,g\,f \ , \tag{5}$$

where $g^{-1} = G^{-1} - \Sigma$ denotes the dressed propagator.

The diagram (d1) shown in Fig. 1 factorizes into two subdiagrams, the first of which is a part of the non-pole scattering kernel of the meson-nucleon T-matrix corresponding to a meson-exchange in the t-channel, while the second subdiagram is the coupling of the intermediate baryon propagator to a pion-nucleon final state. Likewise, the diagram (d2) factorizes into a pion production followed by a subdiagram corresponding to a non-pole meson-baryon scattering kernel. Diagrams (b) and (d) factorize into u-channel processes and pion production amplitudes. The u-channel and t-channel subdiagrams are the Born approximation to the non-pole T-matrix.

In the present work, we restrict the model to the diagrams shown in Fig. 1. This allows a relatively simple treatment of two-pion production because only tree-level diagrams with dressed vertices and dressed propagators taken from a pion-nucleon scattering model have to be evaluated. An iteration of the non-pole subdiagrams would require to solve Eq. (2) which commonly is done numerically relying on a partial wave representation in the center-of-mass frame, but implies technical complications when boosts to other frames are required, e.g. when evaluating the two-pion production amplitude.

In Ref. [23], the inelasticities of the P_{11} partial wave were explained by the final–state interactions, i.e. the non-pole contribution of the T-matrix. In the present model, such a structure cannot be generated. We therefore have to treat the Roper in a simplified way and represent it as

Table 2. Coupling constants and masses in GeV. The constants g_1^2 and g_2^2 are in GeV^{-2}.

$f^2_{\pi NN}/(4\pi)$	0.0778	$f^2_{P11(1440)\pi N}/(4\pi)$	0.011
$f^2_{\pi N\Delta}/(4\pi)$	0.36	$f^2_{P11(1440)\pi\Delta}/(4\pi)$	0.04
$g^2_{\rho NN}/(4\pi)$	0.80	$f^2_{P11(1440)\sigma N}/(4\pi)$	13.0
$\kappa_{\rho NN}$	1.94	$f^2_{D13(1520)\pi N}/(4\pi)$	0.0009
$g^2_{\sigma NN}/(4\pi)$	1.03	$f^2_{D13(1520)\pi\Delta}/(4\pi)$	0.03
$f^2_{\pi\Delta\Delta}/(4\pi)$	0.04	$f^2_{S11(1535)\pi N}/(4\pi)$	0.003
$f^2_{\rho N\Delta}/(4\pi)$	4.5	$f^2_{S11(1535)\eta N}/(4\pi)$	0.47
$g^2_{\rho\Delta\Delta}/(4\pi)$	16.0	$f^2_{S11(1650)\eta N}/(4\pi)$	0.009
$\kappa_{\rho\Delta\Delta}$	15.0		
$g^2_{\rho\pi\pi}/(4\pi)$	2.905	$g_1^2/(4\pi)$	98.94
$g^2_{\sigma\sigma\sigma}/(4\pi)$	0.625	$g_2^2/(4\pi)$	7.32
m_N	0.93893	$m_{D13(1520)}$	1.515
m_Δ	1.232	$m_{S11(1535)}$	1.535
$m_{P11(1440)}$	1.491	$m_{S11(1650)}$	1.701
M_π	0.13803	M_ρ	0.772
M_η	0.5473	M_σ	0.8346

an s-channel resonance. A Roper propagator is introduced which has a structure analogous to the nucleon propagator.

We simplify the formalism employed in Ref. [23] by solving the coupled channel problem for meson-nucleon scattering in the K-matrix approximation. Moreover, we employ a derivative coupling for the coupling of the nucleon resonances to the pseudo-scalar mesons which was used in Ref. [26] to improve the description of the $S_{11}\pi N$ partial wave.

For brevity, we only display the various propagators that enter the calculation. All the necessary formalism to calculate the relevant amplitudes, cross sections etc. can e.g. taken from Ref. [13].

The nucleon propagator is given by:

$$S_N(p) = \frac{\not{p} + m_N}{p^2 - m_N^2 - \Sigma_N(p^2)} \ , \tag{6}$$

with m_N the nucleon mass. The self energy Σ_N is obtained by including the πN, $\pi\Delta$, and the σN reaction channels in Eq. (3). The propagator of the $\Delta(1232)$ is given by

$$D^{\mu\nu}(p) = \frac{\not{p} + m_\Delta}{p^2 - m_\Delta^2 - \Sigma_\Delta(p^2)} (P^{\frac{3}{2}})^{\mu\nu} + D^{\mu\nu}_{\frac{1}{2}} \ , \tag{7}$$

with m_Δ the mass of the $\Delta(1232)$. The spin-1/2 contribution $D^{\mu\nu}_{\frac{1}{2}}$ is identical with the spin-1/2 part of the Rarita-Schwinger propagator. These contributions are, however, non–propagating and can be represented in an effective field theory approach by contact operators, see e.g. [28]. The delta self–energy Σ_Δ is evaluated taking into account only the pion-nucleon intermediate state and neglecting the non-pole contribution of the pion-nucleon interaction, i.e.:

$$\Sigma_\Delta = f_0^\dagger \, G_{\pi N} \, f_0 \ . \tag{8}$$

This is a good approximation because the P_{33} partial wave in the pion-nucleon scattering model of Ref. [23] is given mainly by the Δ-pole diagram for partial waves up to approximately 1.3 GeV.

The interaction Lagrangians employed are shown in Table 1. A partial refit of the parameters of Ref. [23] is required. In a first step, the parameters of the πN potential are readjusted without the N^* pole diagrams to the scattering lengths and phase shifts below 1.2 GeV. Then the $\pi\Delta\Delta$, $\rho N\Delta$, and the $\rho\Delta\Delta$ couplings are fitted. Finally the parameters of the N^* resonances are fixed. Table 2 summarizes the coupling constants and masses. The value of the tensorial ρNN vertex has been reduced in comparison to the value employed in Ref. [23].

The diagrams (d1), (d2), (d3), (d4), and (d5) contain a σ or ρ propagator. Since here we need a reasonable model for the pion-pion interaction below two-pion invariant masses of 1 GeV only, a simplified version of the meson-exchange model to pion-pion scattering suffices [27]. We include a dressing of the σ and ρ propagators by two-pion intermediate states only, neglecting $K\bar{K}$ intermediate states and non-pole scattering kernels. Tables 1 and 2 show the relevant interaction Lagrangian and coupling constants. Unitarity is taken care of by solving Eq. (1) for the two-pion system.

3 Results

In Fig. 2, the threshold behaviour of the total cross sections of the five different experimentally accessible channels

$$\begin{aligned} &\pi^\pm p \to \pi^\pm \pi^+ n \ , \\ &\pi^\pm p \to \pi^\pm \pi^0 p \ , \\ &\pi^- p \to \pi^0 \pi^0 n \ , \end{aligned} \tag{9}$$

are shown as a function of the kinetic energy of the initial state pion in the laboratory frame, T_π. The corresponding invariant mass $\sqrt{s}$ of the initial pion-nucleon system is given by

$$s = (m_N + M_\pi)^2 + 2 m_N T_\pi \ , \tag{10}$$

with M_π the relevant neutral or charged pion mass depending on the channel under consideration. The Δ–isobar corresponds to $T_\pi = 0.19\,\mathrm{GeV}$, while the maximal pion kinetic energy $T_\pi = 0.4$ GeV translates into $\sqrt{s} = 1.38\,\mathrm{GeV}$ which is below the nominal mass of the Roper resonance. The observables are calculated assuming isospin symmetry. Following Refs. [13,15], we included the effect of isospin breaking by the masses of the final states by shifting the isospin symmetric threshold to the correct threshold energy for each reaction channel.

Close to threshold, the present model obtains cross sections which agree with the results of chiral perturbation theory. This could be expected since the model incorporates the experimental information on low energy pion-nucleon scattering. It should be stressed, however, that the model is not as precise as chiral perturbation theory because it does not offer a counting scheme which would

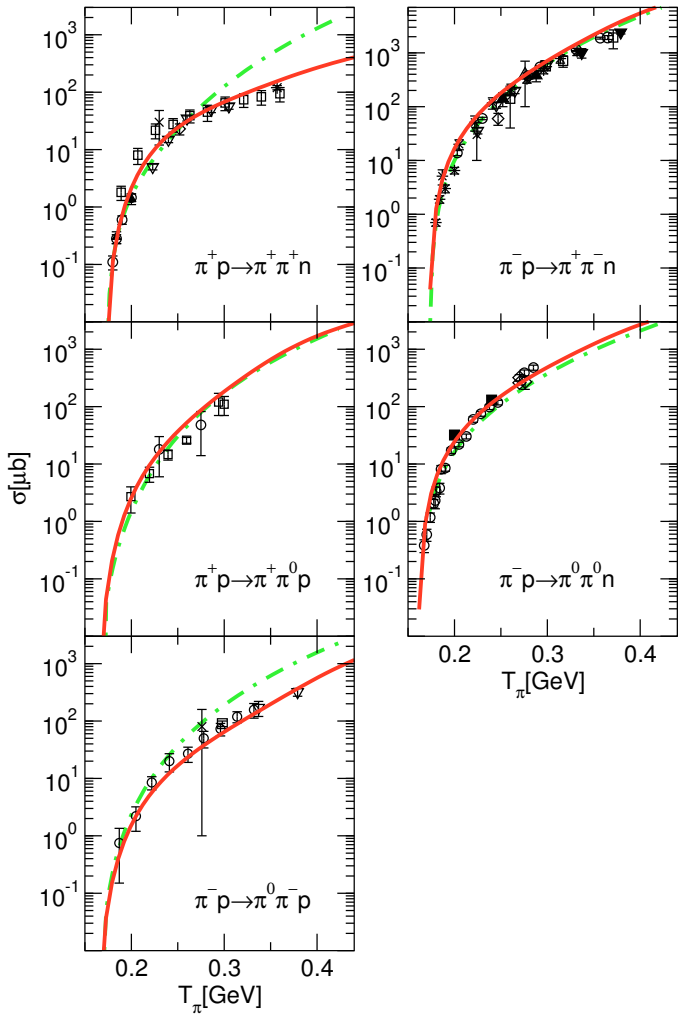

Fig. 2. Total cross sections for the reaction $\pi N \to \pi\pi N$. The (red) solid lines show the results of the present model. For comparison, the results obtained in Heavy Baryon chiral perturbation theory [13] are displayed by the (green) dot-dashed line. The data are taken from Ref. [5] and the compilation in Ref. [29].

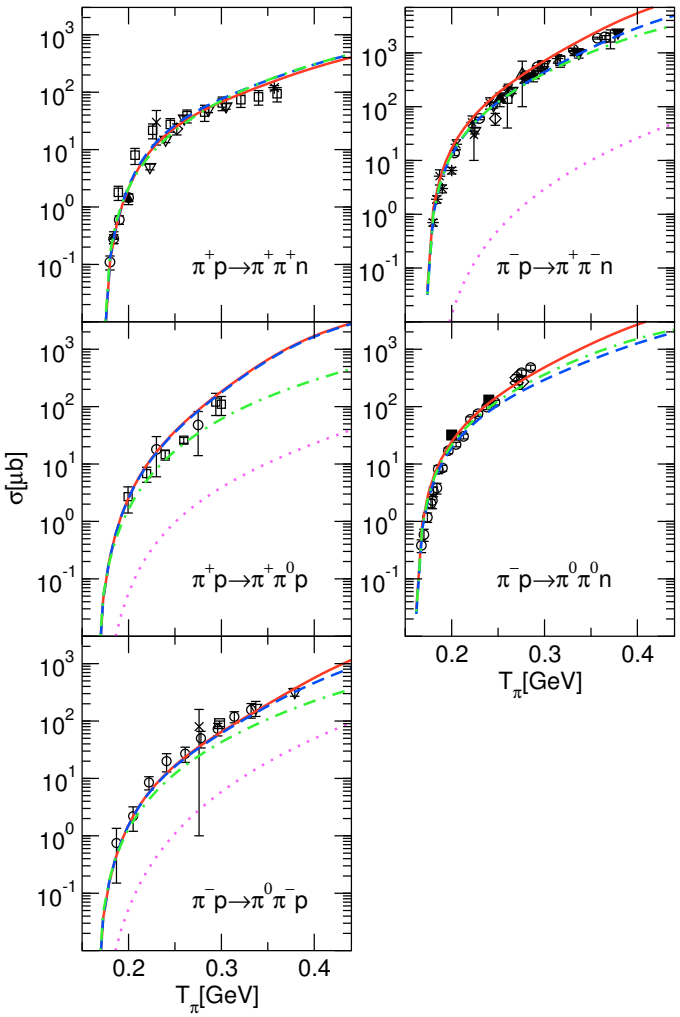

Fig. 3. Influence of resonances on the total cross sections for the reaction $\pi N \to \pi\pi N$. Full model: (red) solid lines; omission of the Δ resonance: (green) dot-dashed lines; omission of the N^* resonances: (blue) dashed lines. The (violet) dotted lines show the contribution of diagrams with an intermediate ρ-meson decaying to two pions.

allow systematic improvements. Chiral perturbation theory starts to overshoot the experimental cross sections for the $\pi^+ p \to \pi^+\pi^+ n$ reaction at about $T_\pi \simeq 0.3$ GeV. Increasing the order of the expansion would push the range of validity of the chiral calculation to higher energies. In the model, some higher order terms are included by unitarization effects. It is important to note that these higher order effects are of no relevance in the threshold region. The model continues to agree with the experimental data up to about $T_\pi \simeq 0.4$ GeV.

In Fig. 3, we investigate the effect of different resonances on the total cross sections by omitting the contribution of various baryon resonances. The Δ-resonance may be expected to play an important role for the $\pi^+ p$ reaction for pion kinetic energies of about $T_\pi = 0.2$ GeV. This is seen in the reaction $\pi^+ p \to \pi^+\pi^0 p$, but not in the reaction $\pi^+ p \to \pi^+\pi^+ n$. A closer inspection showed that the contribution of a diagram with an intermediate Δ resonance by itself is large, but that there is destructive interference between the Δ contributions. Such cancellations are also observed in the description of electromagnetic two-pion production off nucleons in the threshold region, see e.g. [30]. The effect of the Δ can be seen in the $\pi^- p$ reaction channels. The impact of the N^* resonances $S_{11}(1535)$ and $D_{13}(1520)$ on the total cross sections is negligible in each of the five reaction channels in the energy region investigated. The largest effect of N^* resonances is due to the Roper resonance and can be seen in the $\pi^- p \to \pi^+\pi^- n$ and $\pi^- p \to \pi^0\pi^0 n$ reactions, where the two final pions can be produced in a relative s-wave. The role of the Roper was recently also investigated in Ref. [31]. The σN channel is not allowed in the $\pi^- p \to \pi^0\pi^- p$ reaction and therefore the N^* resonances contribute very little.

The model includes two-pion production via an intermediate rho-meson. For the $\pi^+\pi^+ n$ and $\pi^0\pi^0 n$ final

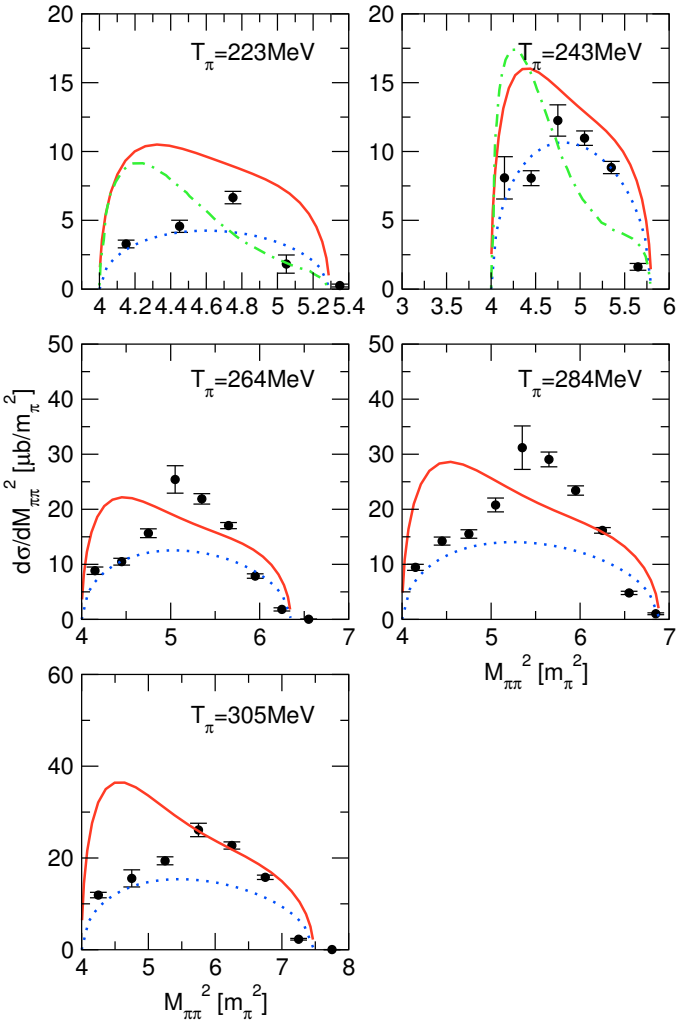

Fig. 4. Differential cross sections $d\sigma/dM^2_{\pi\pi}$ for $\pi^+p \to \pi^+\pi^+n$. Full model: (red) solid line; phase space: (blue) dotted line; chiral perturbation theory: (green) dot-dashed line [13]. The data are from Ref. [5].

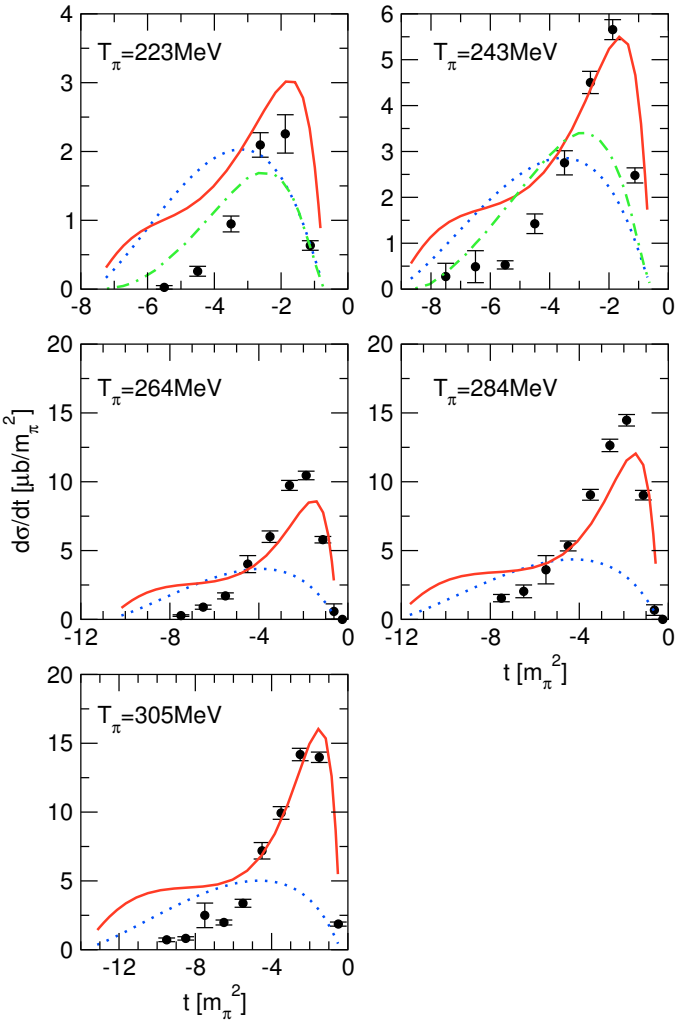

Fig. 5. Differential cross sections $d\sigma/dt$ for $\pi^+p \to \pi^+\pi^+n$. Full model: (red) solid line; phase space: (blue) dotted line; chiral perturbation theory: (green) dot-dashed line [13]. The data are from Ref. [5].

states, trivial isospin selection rules do not allow contributions from an intermediate rho-meson, and in the other final states, the effect of those processes is marginal, as expected, see Fig. 3.

The differential cross sections $d\sigma/dM^2_{\pi\pi}$ for the reactions $\pi^+p \to \pi^+\pi^+n$ are shown for five different values of the kinetic energy T_π of the incident pion in Fig. 4 (here $M_{\pi\pi}$ is the invariant mass of the final-state two-pion system). The data measured at TRIUMF can be fitted reasonably well by three-body phase space [5]. Chiral perturbation theory (CHPT) predicts the average magnitude of the cross sections correctly, but produces a large deviation from phase space emphasizing low values of $M^2_{\pi\pi}$. The cross sections calculated within the resonance model agree with chiral perturbation theory for low values of $M^2_{\pi\pi}$ for both $T_{\pi\pi} = 223$ MeV and $T_{\pi\pi} = 243$ MeV, but drop with increasing $M^2_{\pi\pi}$ more slowly than the CHPT predictions do. For $T_\pi = 305$ MeV, the model reproduces the experimental cross sections above $M^2_{\pi\pi} = 6M^2_\pi$, but overestimates the data below $M^2_{\pi\pi} = 6M^2_\pi$. We note again that the higher order terms generated by the unitarization procedure play only a small role at low energies.

In contrast to the $M_{\pi\pi}$ distributions shown in Fig. 4, the differential cross sections $d\sigma/dt$ strongly deviate from phase space, see Fig. 5. Chiral perturbation theory reproduces the shapes of the t-distributions rather well, but misses the strong rise of the data at small momentum transfers. The model can reproduce the t-distributions nearly quantitatively for small values of the momentum transfer t, but overpredicts the data at large momentum transfers.

The differential cross section $d\sigma/d\cos\theta$ for the $\pi^+p \to \pi^+\pi^+n$ reaction has to be symmetric for $\cos\theta = 0$ because of the symmetry of the reaction under exchange of the two produced pions. The experimental cross sections show a maximum at $\cos\theta = 0$, see Fig. 6. The chiral perturbation theory at order three predicts a minimum, however. The model obtains a maximum near $\theta = 90°$ in qualita-

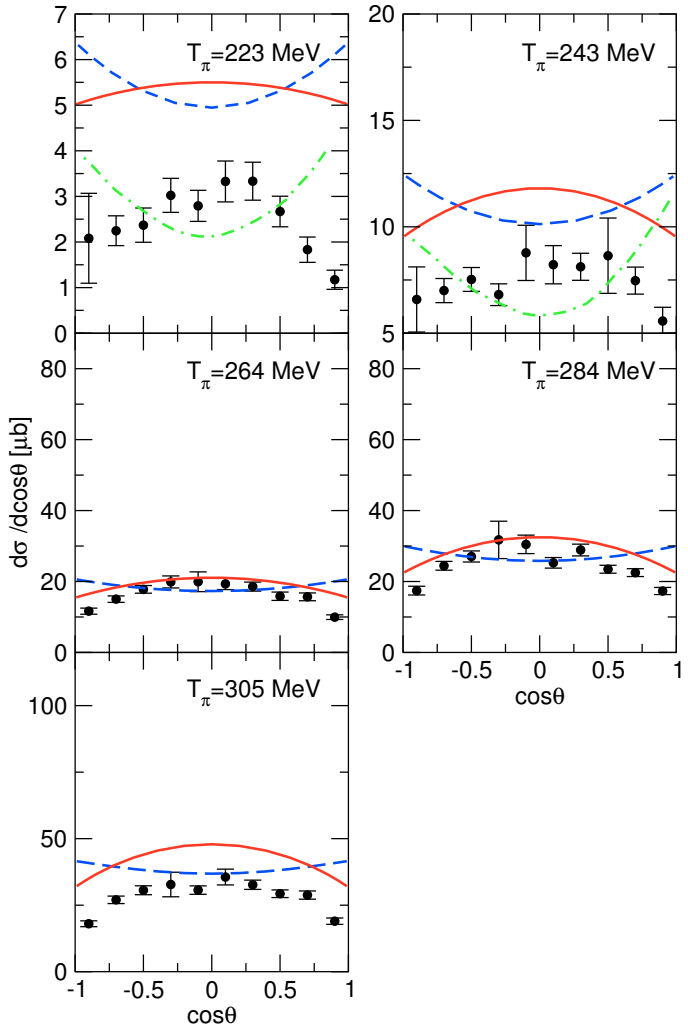

Fig. 6. Differential cross sections $d\sigma/d\cos\theta$ for $\pi^+p \to \pi^+\pi^+n$. Full model: (red) solid line. A calculation employing bare vertices f_0 is displayed by the (blue) dashed line. The predictions of chiral perturbation theory are shown by the (green) dot-dashed line [13]. The data are from [5].

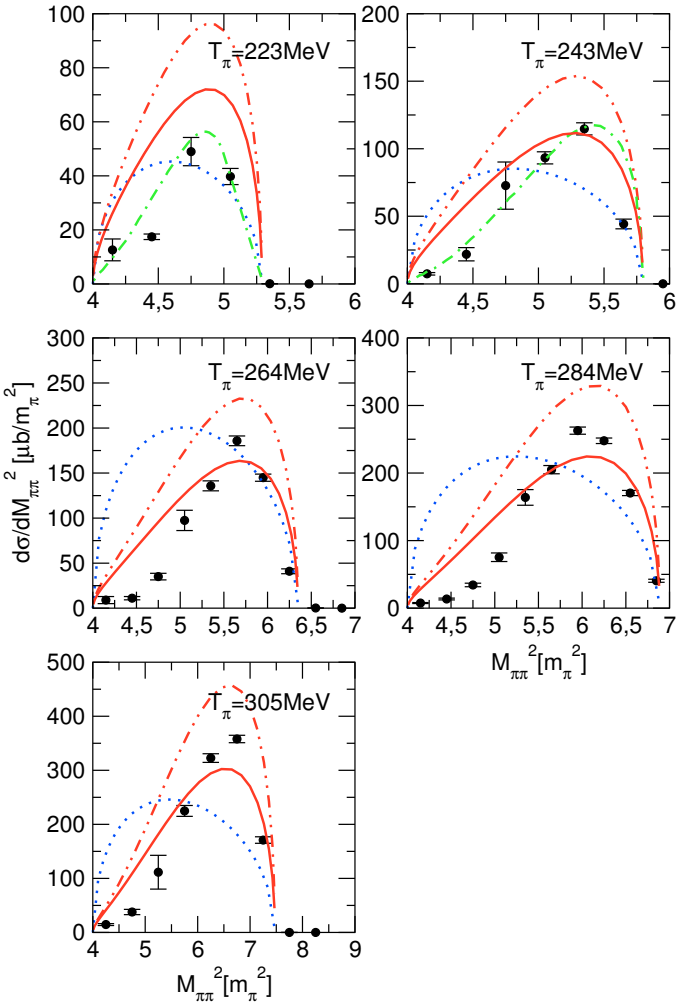

Fig. 7. Differential cross sections $d\sigma/dM^2_{\pi\pi}$ for $\pi^-p \to \pi^+\pi^-n$. Model without Roper resonance: (red) solid line; Model including Breit-Wigner Roper resonance: (red) double-dotted dashed line; phase space: (blue) dotted line; chiral perturbation theory: (green) dot-dashed line [13]. The data are from Ref. [5].

tive agreement with the data. When replacing the dressed vertex functions f by the bare ones, however, the shape of the angular distribution changes and one obtains a minimum at $\theta = 90°$. This finding suggests that a chiral perturbation theory carried to fourth order would solve the problem of the angular distributions in the $\pi^+p \to \pi^+\pi^+n$ reaction.

The differential cross sections $d\sigma/dM^2_{\pi\pi}$ for the reaction for $\pi^-p \to \pi^+\pi^-n$ obtained at TRIUMF are shown in Fig. 7. The experimental data deviate significantly from phase space and show a pronounced maximum close to the largest values of $M^2_{\pi\pi}$. Chiral perturbation theory reproduces the asymmetric distributions very well for the pion kinetic energies $T_\pi = 223$ MeV and $T_\pi = 243$ MeV. The model reproduces the shapes of the distributions, but overestimates the absolute magnitudes. When switching off the contribution from the Roper resonance, however, a reasonable reproduction of the data is achieved. In the present model, we have treated the Roper in a simplified way, which apparently produces an overestimation of the effect of that resonance. If one wants to incorporate the possibility to generate resonances dynamically, a major revision of the present approach is required. In order to include the full non-pole T-matrix, an iteration of the non-pole scattering kernel in the two-pion production diagrams has to be performed for different Lorentz frames. This goes beyond the scope of the tree-level like model discussed here.

4 Summary

We have presented a resonance model for the $\pi N \to \pi\pi N$ reaction which incorporates information from pion–nucleon scattering – these two processes are intimately connected and should not be treated independently from each other. The model is able to reproduce the total cross sections

for kinetic energies of the incident pions up to about 350 MeV for all five reaction channels. This is a success of the present approach which is only partially shared in specific reaction channels by other resonance models which do not include consistently pion-nucleon scattering and two-pion production. The agreement with the differential experimental cross sections is good, though not perfect. The total cross sections have a smooth dependence on the pion kinetic energy which does not allow to deduce obvious information about resonances. The differential cross sections, on the other hand, show characteristic deviations from three-body phase space. The inclusion of the Δ resonance suffices to explain the overall shapes.

In the second resonance region, the model starts to break down. Here, we could trace the difficulties to our approximate treatment of the Roper resonance. The results obtained in the present study suggest to go beyond the Born approximation of the non-pole pion-nucleon T-matrices, when constructing the two-pion production amplitudes for analyses in the second resonance region.

Acknowledgements

We thank Christoph Hanhart for discussions. Partial support from the EU Integrated Infrastructure Initiative Hadron Physics Project (contract no. RII3-CT-2004-506078) and DFG (SFB/TR 16, "Subnuclear Structure of Matter") is gratefully acknowledged.

References

1. R. Fatemi *et al.* [CLAS Collaboration], Phys. Rev. Lett. **91** (2003) 222002 [arXiv:nucl-ex/0306019].
2. W. Langgartner *et al.*, Phys. Rev. Lett. **87** (2001) 052001.
3. M. Wolf *et al.*, Eur. Phys. J. A **9** (2000) 5.
4. S. Prakhov *et al.* [Crystal Ball Collaboration], Phys. Rev. C **69** (2004) 045202.
5. M. Kermani *et al.* [CHAOS Collaboration], Phys. Rev. C **58** (1998) 3419.
6. I. G. Aznauryan, V. D. Burkert, G. V. Fedotov, B. S. Ishkhanov and V. I. Mokeev, Phys. Rev. C **72** (2005) 045201 [arXiv:hep-ph/0508057].
7. A. Anisovich, E. Klempt, A. Sarantsev and U. Thoma, Eur. Phys. J. A **24** (2005) 111 [arXiv:hep-ph/0407211].
8. T. P. Vrana, S. A. Dytman and T. S. H. Lee, Phys. Rept. **328** (2000) 181 [arXiv:nucl-th/9910012].
9. R. A. Arndt, W. J. Briscoe, I. I. Strakovsky and R. L. Workman, Phys. Rev. C **66** (2002) 055213 [arXiv:nucl-th/0205067].
10. L. Tiator, D. Drechsel, S. Kamalov, M. M. Giannini, E. Santopinto and A. Vassallo, Eur. Phys. J. A **19** (2004) 55 [arXiv:nucl-th/0310041].
11. T. Feuster and U. Mosel, Phys. Rev. C **58** (1998) 457 [arXiv:nucl-th/9708051].
12. V. Bernard, N. Kaiser and U.-G. Meißner, Nucl. Phys. B **457** (1995) 147 [arXiv:hep-ph/9507418].
13. N. Fettes, V. Bernard and U.-G. Meißner, Nucl. Phys. A **669** (2000) 269 [arXiv:hep-ph/9907276].
14. N. Mobed, J. Zhang and D. Singh, Phys. Rev. C **72** (2005) 045204.
15. V. Bernard, N. Kaiser and U.-G. Meißner, Nucl. Phys. A **619** (1997) 261 [arXiv:hep-ph/9703218].
16. V. Bernard, N. Kaiser and U.-G. Meißner, Nucl. Phys. A **615** (1997) 483 [arXiv:hep-ph/9611253].
17. T. S. Jensen and A. F. Miranda, Phys. Rev. C **55** (1997) 1039.
18. H. Kammano and M. Arima, Phys. Rev. C **69** (2004) 025206.
19. E. Oset and M. J. Vicente-Vacas, Nucl. Phys. A **446** (1985) 584.
20. O. Jaekel, M. Dillig and C. A. Z. Vasconcellos, Nucl. Phys. A **541** (1992) 675.
21. J. A. Gomez Tejedor and E. Oset, Nucl. Phys. A **600** (1996) 413 [arXiv:hep-ph/9506209].
22. J. C. Nacher, E. Oset, M. J. Vicente and L. Roca, Nucl. Phys. A **695** (2001) 295 [arXiv:nucl-th/0012065].
23. O. Krehl, C. Hanhart, S. Krewald and J. Speth, Phys. Rev. C **62** (2000) 025207 [arXiv:nucl-th/9911080].
24. R. W. Haymaker, Phys. Rev. **181** (1969) 2040.
25. I. R. Afnan and A. T. Stelbovics, Phys. Rev. C **23** (1981) 1384.
26. A. M. Gasparyan, J. Haidenbauer, C. Hanhart and J. Speth, Phys. Rev. C **68** (2003) 045207 [arXiv:nucl-th/0307072].
27. F. P. Sassen, S. Krewald and J. Speth, Phys. Rev. D **68** (2003) 036003 [arXiv:hep-ph/0212056].
28. V. Bernard, T. R. Hemmert and U.-G. Meißner, Phys. Lett. B **565** (2003) 137 [arXiv:hep-ph/0303198].
29. V. V. Vereshagin *et al.*, Nucl. Phys. A **592** (1995) 413 [arXiv:hep-ph/9504361].
30. V. Bernard, N. Kaiser, U.-G. Meißner and A. Schmidt, Nucl. Phys. A **580** (1994) 475 [arXiv:nucl-th/9403013].
31. H. Kamano and M. Arima, arXiv:nucl-th/0601057.